

Article

Combining deep-sequencing, proteomics, phosphoproteomics and functional screens to discover novel regulators of sphingolipid homeostasis

Nicolas Lebesgue, Márton Megyeri, Alba Cristobal, Arjen Scholten, Silvia Gabriela Chuartzman, Yoav Voichek, Richard Alexander Scheltema, Shabaz Mohammed, Anthony H. Futerman, Maya Schuldiner, Albert J.R. Heck, and Simone Lemeer

J. Proteome Res., **Just Accepted Manuscript** • DOI: 10.1021/acs.jproteome.6b00691 • Publication Date (Web): 14 Nov 2016

Downloaded from <http://pubs.acs.org> on November 15, 2016

Just Accepted

"Just Accepted" manuscripts have been peer-reviewed and accepted for publication. They are posted online prior to technical editing, formatting for publication and author proofing. The American Chemical Society provides "Just Accepted" as a free service to the research community to expedite the dissemination of scientific material as soon as possible after acceptance. "Just Accepted" manuscripts appear in full in PDF format accompanied by an HTML abstract. "Just Accepted" manuscripts have been fully peer reviewed, but should not be considered the official version of record. They are accessible to all readers and citable by the Digital Object Identifier (DOI®). "Just Accepted" is an optional service offered to authors. Therefore, the "Just Accepted" Web site may not include all articles that will be published in the journal. After a manuscript is technically edited and formatted, it will be removed from the "Just Accepted" Web site and published as an ASAP article. Note that technical editing may introduce minor changes to the manuscript text and/or graphics which could affect content, and all legal disclaimers and ethical guidelines that apply to the journal pertain. ACS cannot be held responsible for errors or consequences arising from the use of information contained in these "Just Accepted" manuscripts.



ACS Publications

Combining deep-sequencing, proteomics, phosphoproteomics and functional screens to discover novel regulators of sphingolipid homeostasis

Nicolas Lebesgue^{†‡#}, Márton Megyeri^{§¶}, Alba Cristobal^{†‡}, Arjen Scholten^{†‡}, Silvia G. Chuartzman[§], Yoav Voichek[§], Richard A. Scheltema^{†‡}, Shabaz Mohammed^{†‡δ}, Anthony H. Futerman[¶], Maya Schuldiner^{§*}, Albert J.R. Heck^{†‡} and Simone Lemeer^{†‡*}.

[†]Biomolecular Mass Spectrometry and Proteomics, Bijvoet Center for Biomolecular Research and Utrecht Institute of Pharmaceutical Sciences, Utrecht University, Padualaan 8, 3584 CH Utrecht, The Netherlands.
[‡]Netherlands Proteomics Center, Padualaan 8, 3584 CH Utrecht, the Netherlands.
[§]Department of Molecular Genetics, Weizmann Institute of Science, Rehovot 7610001, Israel.
[¶]Department of Biological Chemistry, Weizmann Institute of Science, Rehovot 7610001, Israel.
^δCurrent address: Janssen Infectious Diseases and Vaccines, Crucell Holland B.V., Leiden, the Netherlands.
^δCurrent address: Departments of Chemistry and Biochemistry, University of Oxford, Physical & Theoretical Chemistry Laboratory, South Parks Road, OX1 3QZ Oxford, United Kingdom.

[#]These authors contributed equally to this work
^{*}To whom correspondence should be addressed. E-mail: maya.schuldiner@weizmann.ac.il or s.m.lemeer@uu.nl

Key words: sphingolipid metabolism, *Saccharomyces cerevisiae*, proteomics, phosphorylation, label-free quantification, mass spectrometry, myriocin

ABSTRACT

Sphingolipids (SLs) are essential components of cell membranes and are broad-range bioactive signaling molecules. SL levels must be tightly regulated as imbalances affect cellular function and contribute to pathologies ranging from neurodegenerative and metabolic disorders to cancer and aging. Deciphering how SL homeostasis is maintained and uncovering new regulators is required for understanding lipid biology and for identifying new targets for therapeutic interventions. Here we combine omics technologies to identify the changes of the transcriptome, proteome and phosphoproteome in the yeast *Saccharomyces cerevisiae* upon SL depletion induced by myriocin. Surprisingly, while SL depletion triggers important changes in the expression of regulatory proteins involved in SL homeostasis, the most dramatic regulation occurs at the level of the phosphoproteome suggesting that maintaining SL homeostasis demands rapid responses. To discover which of the phosphoproteomic changes are required for the cell's first-line response to SL depletion we overlaid our omics results with systematic growth screens for genes required during growth in myriocin. By following the rate of SL biosynthesis in those candidates that are both affecting growth and are phosphorylated in response to the drug, we uncovered Atg9, Stp4 and Gvp36 as putative new regulators of SL homeostasis.

INTRODUCTION

Sphingolipids (SLs) are structural components of cell membranes as well as signaling molecules involved in a wide range of cellular processes including secretion, endocytosis, chemotaxis, neurotransmission, angiogenesis, and inflammation¹. Over the past years, significant new insights on SL metabolism have emerged, including delineating the compartmentalized synthesis of SLs in the endoplasmic reticulum (ER) and the Golgi apparatus as well as SL trafficking, turnover and degradation^{1,2}. However, the regulation of SL homeostasis in response to metabolic demand remains largely unexplored^{3,4}. SL metabolites have been implicated in the onset and progression of various diseases including cancer, lung diseases, diabetes, and lysosomal storage disorders⁵. Thus, understanding the complexity of SL metabolism and the intricacies of its regulation is essential to define proper key sites for potential therapeutic intervention. The budding yeast *Saccharomyces cerevisiae* is an ideal model system to study eukaryotic lipid metabolism due to the high conservation as well as ease of use for systematic studies⁶. Studies in yeast have enabled the identification of key enzymes and sensors regulating SL metabolism in all eukaryotes, including mammals⁶.

The first and rate-limiting step in the *de-novo* synthesis of SLs is common to mammals and yeast and takes place on the cytosolic face of the ER by the condensation of serine and palmitoyl-CoA. This condensation leads to the synthesis of 3-ketosphinganine via the heterodimeric enzyme, serine palmitoyltransferase (SPT)⁷. SPT is composed of two subunits in yeast (Lcb1/Lcb2) and is embedded in the SPOTS protein complex with its regulators Orm1/2, Tsc3 and Sac1⁸. The role of the ORM proteins in this complex is to act as negative regulators of SPT. ORMs are constitutive members of the complex, consequently their activation and repression is not mediated by their expression pattern but rather by their phosphorylation state⁸. Specifically, when SL levels drop,

such as in the presence of the SPT inhibitor myriocin, the ORM proteins are reversibly phosphorylated by the Ypk1 kinase, inhibiting their activity and consequently removing the inhibition of SPT activity. Hence, Ypk1 phosphorylation indirectly activates SPT and increases the synthesis of SL precursors, creating a feedback loop⁹. The ORM mediated feedback loop is an example of how SL dynamics can be regulated by reversible protein phosphorylation. It is well known that additional phosphorylation events occur in key enzymes in the pathway^{10,11}. However, to date, the exact extent of protein phosphorylation in response to changes in SL homeostasis as well as additional roles, are unknown. More generally, the network of regulatory proteins acting at the various levels of SL biosynthesis, inter-conversion and breakdown is far from being understood.

Here, we combined deep sequencing, mass spectrometry based proteomics and phosphoproteomics, along with whole-genome functional screens to identify regulatory proteins controlling SL biosynthesis in *Saccharomyces cerevisiae* following depletion of SLs by myriocin treatment. Using metabolic labeling assays for *de novo* formation of SLs we validated the involvement of three new regulators: Atg9, Stp4 and Gvp36. Globally, our multi-pronged approach permitted identification of new, unstudied proteins as modulators of SL homeostasis and suggests that the regulatory system of SLs is highly responsive, extremely dynamic and much more complex and intricate than previously thought.

EXPERIMENTAL SECTION

Yeast media and growth conditions

Yeast cells were either grown in rich liquid media, YPD (Yeast extract, Peptone, Dextrose) (1% Bacto-yeast extract (BD), 2% Bacto-peptone (BD) and 2% dextrose (Amresco)) or synthetic liquid medium, SD (Synthetic Defined) (0.67% yeast nitrogen base with ammonium sulfate and without amino acids (CondaPronadisa) and 2% dextrose (Amresco) supplemented with amino acids (Amresco)). Agar plates also included 2.2% agar. Upon screening the overexpression library, SGal complete agar plates were used (similar to SD complete medium where the 2% dextrose was replaced with 2% galactose (Amresco)). In this study all the strains were grown at 30°C.

Strains used in this study

The yeast strain used for transcriptome, proteome and phosphoproteome analysis was SEY6210 (MAT α *ura3-52 his3- Δ 200 leu2-3,112 trp1- Δ 901 lys2-801 suc2- Δ 9*). In the functional screens we used whole-genome mutant library (consisting of ~5000 non-essential deletions¹² and ~1000 hypomorphic alleles of essential genes¹³) or an overexpression library^{14,15}. Strains harboring deletion for *GVP36*, *ATG9* and *STP4* were taken from the deletion library¹².

Cell culture and mRNA extraction for transcriptome analysis

The yeast strain SEY6210 was grown overnight in YPD. Two samples were back diluted in YPD to let the yeast reach logarithmic phase. At OD₆₀₀=0.8 the YPD medium was supplemented with two different final concentrations of myriocin from *Mycelia sterilia* (Sigma) (150 ng/ml and 300 ng/ml, respectively). 1.5 ml of samples were taken at 0 and 60 min, spun down at 4 °C and frozen

1
2
3 in liquid nitrogen. RNA was extracted as described¹⁶ using Nucleospin 96 RNA kit. Cell lysis
4 was done in a 96-well plate by adding 450 µl of lysis buffer containing 1 M sorbitol (Sigma-
5 Aldrich), 100 mM EDTA, and 0.45 µl lyticase (10 IU/µl). The plate was incubated at 30°C for
6
7
8 30 s in order to break the cell wall and then centrifuged for 10 s at 2500 rpm, and the supernatant
9
10 was transferred to a new 96-well plate that was provided by the Nucleospin 96 RNA kit. From
11
12 that stage on, the extraction continued using this kit. From RNA extracts, cDNA was made for
13
14 each sample. The cDNA samples were run in the Illumina Highseq 2500.
15
16
17
18
19
20
21
22

23 **RNA sequencing analysis**

24
25 RNA reads were aligned to the yeast strain S288C R64 reference genome with BOWTIE¹⁷.
26
27 Number of reads for each gene was normalized by the total number of reads and multiplied by
28
29 10^6 . Genes that obtained below ten normalized reads were discarded from the analysis. After
30
31 alignment to the genome the read number per sample was calculated for every gene. The raw data
32
33 was compiled by using a script written in matlab. The fold changes of the mean (of two repeats)
34
35 of the two time points were compared, then sorted and plotted for each condition in \log_2 scale.
36
37 Hits were defined as those with signal larger than 2 (upregulated) or less than 0.5
38
39 (downregulated). The hits were compared with SL homeostasis genes (Supplementary table 1)
40
41 and with genes related to the general stress response¹⁸. The analysis was done in Rstudio. The
42
43 raw data were submitted to the ENA database (study number: PRJEB16833)
44
45
46
47
48
49
50
51
52
53
54
55
56
57
58
59
60

Cell culture for proteome and phosphoproteome studies

The yeast strain SEY6210 was grown in YPD medium to early/mid-log phase ($OD_{600}= 0.8$). Medium was supplemented with 150 ng/ml of myriocin from *Mycelia sterilia* (Sigma) or ethanol. Cells were harvested after 0, 30, 60, 120 and 180 min of treatment by gentle centrifugation at $3000 \times g$ for 10 min at 4 °C. Cell pellets were washed twice with milliQ water and snap-frozen in liquid nitrogen. Frozen cell pellets were freeze dried overnight and the remaining powder stored at -80 °C prior cell lysis.

Cell lysate for proteome and phosphoproteome studies

10 mg of yeast powder was resuspended in 100 µl of lysis buffer (8 M urea, 2 M thiourea, 50 mM Ammonium bicarbonate containing protease inhibitors (complete-Mini EDTA free, Roche) and Phosphatase inhibitor (PhosSTOP, Roche)). Cells were disrupted with 0.5 mm diameter glass beads (Biospec products) (volume: beads ratio = 1) using a Tissue Lyser II (QIAGEN) for 5 min at 4°C. Supernatant was collected and remaining glass beads were washed with 600 µl of lysis buffer, vortexed 10 to 15 seconds. The second supernatant was collected and combined with the first one leading to a total volume of approximately 800 µl. Lysates were centrifuged 15 min at 20000 rpm at 4 °C and protein content in the supernatant was determined using Bradford assay (Biorad).

Protein digestion for proteome and phosphoproteome studies

Proteins were reduced by addition of 5 mM DTT and incubated for 35 min at 55 °C. The mixture was cooled to room temperature, followed by alkylation using 15 mM iodoacetamide in the dark for 25 min. The alkylation reaction was quenched with 5 mM dithiothreitol. A first proteolytic

1
2
3 digestion was performed by addition of Lys-C (Wako Chemicals) during 4h at 37°C, 1:75
4 enzyme to protein ratio concentration. Urea concentration was diluted to 2 M with 50
5 mM ammonium bicarbonate (AMBIC) pH 8.0. Second proteolytic digestion was performed by
6 addition of Trypsin (Promega), 1:100 enzyme to protein ratio, and incubated at 37 °C overnight.
7
8 The digestion was quenched by addition of 10% formic acid (FA) and desalted over a C18 Sep-
9 Pak (Waters). Eluted peptides were finally dried down and stored at -80 °C.
10
11
12
13
14
15
16
17
18
19

20 **Phosphopeptide purification by immobilized titanium (IV) ion IMAC adsorbents**

21
22 IMAC material was prepared and used as previously described¹⁹. Briefly, Gel-loader tips that
23 were plugged with C8 material (3M) were filled up to 1 cm with Ti⁴⁺-IMAC beads. Columns
24 were equilibrated with 50µl loading buffer (80% ACN, 6% trifluoroacetic acid (TFA)). 200 µg of
25 peptides were reconstituted in 100 µl loading buffer, loaded onto the columns and washed with
26 50µl washing buffer 1 (50% acetonitrile (CAN), 0.5% TFA, 200 mM NaCl) and subsequently 50
27 µl washing buffer 2 (50% ACN, 0.1% TFA) at 50 × g at 4 °C. Phosphopeptides were eluted with
28 35 µl elution buffer 1 (10% NH₃ in H₂O) followed by 2 µl elution buffer 2 (80% ACN, 2% FA) at
29 50 × g at 4°C. Eluate was acidified with 3 µl 100% FA, dried down and stored at -80 °C until
30 analysis by Nanoscale liquid chromatography coupled to tandem mass spectrometry (LC-
31 MS/MS)
32
33
34
35
36
37
38
39
40
41
42
43
44
45
46
47
48

49 **Liquid chromatography and mass spectrometry**

50
51 LC-MS/MS was performed in technical duplicate on a reversed-phase EASY nano-LC 1000
52 (Thermo Fisher Scientific) coupled to an Orbitrap Q-exactive mass spectrometer (Thermo
53 Scientific) using higher-energy collisional dissociation (HCD) fragmentation. Briefly, peptides
54
55
56
57
58
59
60

were loaded on a double-fritted trap column (100 μm inner diameter x 2cm, packed with 3 μm C18 resin, ReproSil-Pur AQ; Dr. Maisch) at a flow rate of 5 $\mu\text{l}/\text{min}$ in 100% buffer A (0.1% FA in water). Peptides were transferred to an analytical column (50 μm inner diameter x 50 cm, packed with 2.7 μm C18 particles, Poroshell 120 EC-C18; Agilent Technologies) and separated using a 180 minutes gradient from 7 to 30% buffer B (0.1% FA in 100% ACN) at a flow rate of 100 nl/min. Q-exactive survey scans were acquired at 35,000 resolution to a scan range from 350 to 1500 m/z. The mass spectrometer was operated in a data-dependent mode to automatically switch between MS and MS/MS. The twenty most intense precursor's ions were submitted to HCD fragmentation using an MS/MS resolution set to 17,500, a precursor automatic gain control (AGC) target set to 5×10^4 , a precursor isolation width set to 1.5 Da, and a maximum injection time set to 120 ms.

Data processing for proteome and phosphoproteome studies

Raw data were processed with MaxQuant version 1.3.0.5²⁰. MS and MS/MS spectra were searched using the Andromeda search engine against a *Saccharomyces* Genome Database version 2010_02 containing 5779 proteins. The database search was performed with the following parameters: Methionine oxidation, S,T,Y phosphorylation set as variable modification for the phosphopeptide analysis, cysteine carbamidomethylation set as fixed modification, max charge peptide = 6, minimum peptide length = 6, FT MS/MS tolerance = 0.05Da, peptide and protein identification set to 1% FDR. For label-free quantification (LFQ), match between runs was selected with a maximum shift time window of 3 minutes. The mass spectrometry proteomics data have been deposited to the ProteomeXchange Consortium²¹ via the PRIDE partner repository with the dataset identifier PXD003463. Proteins and phosphopeptides that were only identified by reverse hits or identified as contaminants were filtered out from the resultant peptide

list generated by MaxQuant. Proteins and phosphosites were quantified by label-free quantification. Normalization was performed by subtracting the median of log transformed intensities for each nLC-MS/MS run. Proteins and phosphosites were considered as quantified if detected in at least 2 biological replicates in treated and control conditions and in at least one time point. To identify significantly regulated proteins, a two sample t-test was performed and proteins were defined as regulated with at least 2 fold changes and a p-value ≤ 0.05 between treated and control conditions in at least one time point. To identify significantly regulated phosphorylation sites, statistical validation was performed using a two sample t-test with a permutation-based FDR. Phosphorylation sites with at least 4 fold changes between treated and untreated conditions and a q-value ≤ 0.2 in at least one time point were considered as significantly regulated prior cluster analysis using R.

Myriocin screening on the yeast deletion and overexpression libraries

The yeast deletion¹² and DaMP (hypomorphic alleles)¹³ libraries were replicated on SD and the yeast overexpression library^{14,15} was plated on SGal agar plates. All libraries were incubated with or without myriocin (0,05 $\mu\text{g/ml}$) at 30°C and were imaged after 36 h. Colony sizes were analyzed using the Balony²² software.

Metabolic labeling of yeast strains

Radioactive [4,5 ³H]-dihydrosphingosine was prepared as described previously²³ and was further purified in chloroform:methanol:2M acetic acid (18:10:2) before use in the metabolic labeling experiments. The OD of 1 ml cell culture of the different yeast strains in early logarithmic phase were adjusted to 0.3 in SD complete medium and then cells were incubated with or without

myriocin (1 μg/ml) for 10 min before the labeling. Then 8 μCi of [4,5 ³H]-dihydrosphingosine were added and cells were incubated for 30 min. To terminate the reaction cells were placed on ice and 50 μl of NaN₃ (10% in water) were added. Cell pellets were washed with 1 ml of ice-cold water and lipids were extracted by the addition 500 μl of chloroform-methanol-water (CMW) (10:10:3) by vortexing with 200 μl glass beads as described previously²⁴. Cell debris was separated by centrifugation and the organic phase was transferred to a new tube and dried under nitrogen flow. Dried samples were dissolved in 100 μl of water-saturated n-butanol and extracted with 50 μl of water. The aqueous phase was back extracted twice with 100 μl of water-saturated n-butanol. The combined butanol phase was dried under nitrogen flow and dissolved in 30 μl of CMW and then applied to thin layer chromatography plates (Kieselgel 60 plates, 20 X 20; Merck Millipore) and developed in a chloroform:methanol:2M acetic acid (18:10:2) solvent system as described²⁵. Radiolabeled lipids were exposed to a tritium-sensitive screen (BAS-IP TR 2025 E, GE Healthcare Life Sciences) for 8h, visualized and quantified on a Bio-Rad phosphorimager.

RESULTS

Inhibition of SL biosynthesis by myriocin rewires the core pathway to maintain the levels of long chain bases

In order to understand how cells respond to a slowdown in SL biosynthesis we inhibited SPT by a low dose of myriocin and performed transcriptomic, proteomic, phosphoproteomic and functional analyses to uncover novel regulators under these conditions (**Figure 1A**). First, we performed the transcriptomic analysis using two concentrations of myriocin (**Figure S-1**) that are known to inhibit SPT (myriocin has nanomolar affinity to Lcb1/Lcb2²⁶), but minimally affect growth or viability during the 60 min treatment (150 ng/ml or 300 ng/ml) (**Figure S-2 and S-3**). This

ensures the identification of factors responsible for the response to myriocin and not to cell cycle arrest or death.

Following administration of myriocin we quantified and annotated 4,888 and 4,938 transcripts for the two different concentrations of treatment (YPD+150 ng/ml and YPD+300 ng/ml, respectively) (**Figure 1B**). While a variety of transcripts were up or down regulated, we focused on transcripts of known SL enzymes and regulators (**Figure 1C** and **Table S-1**). Interestingly, affected transcripts, either going up or down, seem to play a central role in minimizing the loss of Long Chain Bases (LCBs) (both the dihydrosphingosine (DHS) and the phytosphingosine (PHS) forms), which are central metabolites whose levels must be tightly maintained. For example, Ydc1 and Ypc1, ceramidases that produce DHS and PHS, are upregulated. Similarly Dpp1, a phosphatase converting LCB-phosphates into LCBs, is also upregulated at the 150 ng/ml myriocin treatment. On the other hand the LCB kinase, Lcb5, which reduces the conversion of LCBs to their phosphorylated isoforms, is downregulated at 150 ng/ml treatment. Hence when there is less *de novo* synthesis of LCBs, their levels are maintained by changing the flux of the SL pathway (**Figure 1B** and **Figure 1C**).

Interestingly, the transcriptional rewiring suggests that there is precise information on where the pathway is blocked: Faa4, which provides the substrate for the SPT complex by converting palmitic acid to palmitoyl-CoA, is downregulated. This is despite the fact that Hfd1, which catalyses the conversion of hexadecanal into palmitic acid, is upregulated (**Figure 1B** and **Figure 1C**).

With a more global survey, we find that the number of transcripts that were down or upregulated at least two fold, increased in a dose dependent manner (518 and 740 transcripts, respectively) (**Figure 1D**). Among these regulated transcripts there were 201 and 293 genes (150 ng/ml and 300 ng/ml, respectively) that have been assigned to the general stress response¹⁸. Interestingly,

1
2
3 increasing the myriocin dose (300 ng/ml) increases the general stress response of the cell (**Figure**
4 **1D**) while reducing the extent of regulated changes in the SL metabolic pathway. For example
5
6 Dpp1 and Lcb5 are not regulated at 300ng/ml as opposed to treatment with 150 ng/ml (**Figure**
7 **1B**). After extracting the general stress response genes and the known SL modulators, there were
8
9 still hundreds of changes occurring at the level of the transcriptome. To uncover which of these
10
11 were important for regulatory purposes, we continued to investigate whether these transcripts
12
13 were also affected on the protein level. For these experiments the 150 ng/ml myriocin treatment
14
15 condition was used as it elicits a more focused SL response instead of a broad stress response.
16
17
18
19
20
21
22
23
24
25

26 **Changes in kinases and phosphatases occur during early time points following inhibition of**
27 **SL biosynthesis.**
28
29

30
31 To correlate the changes at the transcriptional level with changes at the proteome level we
32
33 performed in-depth quantitative proteomic analysis of yeast treated with myriocin over several
34
35 time points (**Figure 2A**). We extended our analysis beyond the original 60 min treatment to allow
36
37 transcriptional changes to be manifested as changes at the proteome level. Our method²⁹ (**Figure**
38 **2A**) identified a total of 3,286 unique proteins with less than 1% false discovery rate (FDR). Of
39
40 these, 2,845 unique proteins were quantified in at least 2 out of 3 biological replicates and in at
41
42 least one time point. A total of 563 unique proteins changed significantly when looking at all time
43
44 points (Log_2 fold change ≥ 1 ; $p\text{-value} \leq 0,05$) corresponding to 20% of the quantified proteins.
45
46 Interestingly, most of the proteins whose levels changed significantly did not change at the early
47
48 time-points. Only 101, 94 and 114 unique proteins changed in abundance at 5, 30 and 60 min
49
50 from initiation of myriocin treatment, representing only 8% of the quantified proteins (**Figure**
51 **2B**). The majority, therefore, changed only 3 hours following myriocin treatment with 175 and
52
53
54
55
56
57
58
59
60

385 unique regulated proteins at 120 min and 180 min respectively (**Figure 2B**). These late changes most likely do not represent a cellular response to restore homeostasis, but rather secondary events that occur as cells start to die (Supplementary Figure S3) after 180 min of SL depletion.

Of 38 proteins with known roles in the SL metabolic pathway (**Figure 1C**), 15 were quantified successfully in both the transcriptomic and proteomic analysis after 60 min of myriocin treatment (**Table S-1 and S-2**). From these, the vast majority (10 proteins) did not change in protein abundance (**Figure 1C and Figure 2C**) in agreement with the transcriptomic data (**Tables S-1 and S-2**). However, for those that did change we saw consistency between the two approaches. The serine palmitoyl transferase subunit, Lcb2 (\log_2 ratio=1.06, $-\log_{10}$ p-value=1.67), displayed increased levels, potentially to downregulate the ceramide synthases and maintain LCB levels. Similarly, the SL alpha-hydroxylase, Scs7, showed reduced abundance (\log_2 ratio=-1.27, $-\log_{10}$ p-value=2.21) leaving more ceramide that can be converted to free LCBs (**Figure 2C**).

To study the SL pathway more closely we profiled the temporal changes of the main SL enzymes enabling us to observe expression trends for specific proteins, even if the change at any single time point was not strongly significant (**Figure 2D**). For example Lcb2 was significantly upregulated at a single time point, however two additional members, Lcb1 and Sac1, demonstrated consistent increase in abundance from 60 min of treatment until 180 min of treatment similarly to Lcb2. In addition we see a consistent downregulation of Tsc10, the enzyme downstream to SPT, consistent with the depletion of its substrate in myriocin treated cells (**Figure 2D**).

To try and zoom in on what happens as the first-line of defense we shifted our attention to the earliest time points. Intriguingly, in the small number of proteins with significant changes in their

abundance level in the first hour of treatment, many kinases and phosphatases were identified (Figure S-4). For example, Pho85, a kinase that inhibits the sphingoid long chain base kinase Lcb4²⁷, was significantly upregulated over the entire time course of treatment. Conversely, the protein kinase, Pkc1, was downregulated significantly as early as 30 minutes after treatment (\log_2 ratio=-3.19 and continuously until 180 min of treatment (\log_2 ratio=-2.17)). Previously it has been shown that Pkc1 is activated by SL stress, for example during a transient increase of LCBs upon heat shock²⁸. In agreement, a reduction of Pkc1 as we have observed, should contribute to the release of its inhibitory function. More generally, the small number of proteins whose abundance changes in the early time points following myriocin treatment, coupled with the significant changes in kinases and phosphatases suggested that SL biosynthetic processes may be initially controlled by phosphorylation mediated signaling pathways.

Depletion of SLs has dramatic effects on the yeast phosphoproteome

To decipher which regulatory network acting to maintain SL homeostasis was wired through phosphoproteomic changes, and to reveal potential signaling pathways affecting SL metabolism, we performed an in-depth and sensitive yeast phosphoproteome analysis. To ensure large scale and high throughput quantification of phosphorylation dynamics we used the label free Ti^{4+} -IMAC (Immobilized Metal Ion Affinity Chromatography) enrichment strategy²⁹ at 5, 30, 60, 120 and 180 min following myriocin treatment (Figure 2A). In total, 11,227 unique phosphorylation sites were identified with a maximum of 1% FDR identification. Phosphosites were quantified if the MS1 intensity of the corresponding phosphopeptide was measured in at least 2 biological replicates and in at least one time point, leading to a total of 6,219 unique quantified phosphorylation sites (Table S-3). Since protein phosphorylation is a highly dynamic process, we

1
2
3 focused on the most significant changes that occurred. We found 996 unique phosphorylation
4
5 sites corresponding to 572 unique phosphoproteins that displayed a minimum of 4 fold change
6
7 between treated and untreated conditions and had a significant q-value ≤ 0.2 in at least one time
8
9 point. More than 90% of those phosphorylation sites were localized with a minimum site
10
11 localization probability of 0.75 in a singly, doubly or triply phosphorylated peptide (**Table S-3**).
12

13
14 In this strictly defined differential category, we observed many changes previously documented
15
16 in the literature. For example, Orm1 phosphorylation sites S29, S32, S35 and S36 displayed a
17
18 continuous increase in phosphorylation, in agreement with previous reports³⁰ (**Figure 3A**). These
19
20 sites were previously implicated in activating the synthesis of complex SLs via the TORC1
21
22 pathway, independently of SPT activity³⁰. Indeed here we show that these sites are
23
24 phosphorylated also upon myriocin treatment. Another known change occurs in Ypk1/2, which is
25
26 activated upon changes in SL levels^{9,10,31}. We identified and quantified Ypk1 phosphorylation
27
28 sites S63, S653 and S672 (**Figure 3A**). Out of these sites only S653 has previously been
29
30 implicated in the synthesis of complex SLs³² suggesting that the two additional sites represent an
31
32 additional level of regulation. Lastly, Ypk2 T501 phosphorylation (**Figure 3A**) that has been
33
34 reported to be activated upon rapamycin treatment via the TORC2 pathway, was found to be
35
36 upregulated³³.
37
38
39
40
41
42

43
44 Using these known phosphorylation changes as a validation of our approach, we next focused on
45
46 the novel sites that we observed. Despite the application of stringent thresholds, hundreds of
47
48 phosphosites still remained. To try and organize them into coherent groups we divided the
49
50 regulated sites into six distinct time profiles generated with a Euclidian distance algorithm
51
52 (**Figure 3B**). Indeed, these time profile clusters highlighted three groups with regulation at a
53
54
55
56
57
58
59
60

single time-point (early, median or late) as well as those phosphosites that are continuously and progressively reduced or increased.

GO analysis on the cluster that showed phosphosites regulated at a single, early, time point (“downregulation at 30 min”) we found an enrichment of proteins related to the mitogen-activated protein kinase (MAPK) signaling cascade, including the kinases Bck1, Ssk2 and Cla4 (**Figure 3C** and **Table S-4**). Recent reports suggested that the MAPK signaling cascade is activated by disruption of SL homeostasis³⁴. Our data suggests that these kinases are indeed regulating early signaling events after SL depletion.

Focusing on the clusters of proteins regulated at a single, median, time point (e.g. 60 min) we could see that they are enriched for proteins with a role in phospholipid transport, including the kinases Ypk1 and Fpk1 (**Figure 3C** and **Table S-4**). Interestingly, those kinases are known to be involved in TORC2 dependent control of Orm proteins. Indeed our data shows an increased phosphorylation on multiple sites of these kinases over the entire time of treatment, independently of their protein abundance (**Table S-3**)⁹.

Another process that is enriched at early time points is vesicular mediated transport (and specifically ER to Golgi trafficking through COPII vesicles) (**Figure 3C** and **Table S-4**). Ceramides themselves have to be trafficked between the ER and Golgi and it has already been shown that SLs affect ER to Golgi trafficking³⁵. Our data suggests that an important effector of this crosstalk is Sec16, an enigmatic regulator of COPII vesicle formation, as Sec16 is phosphorylated at 11 different sites upon SL depletion (**Figure S-5** and **Table S-4**). The lipid transfer proteins, Osh2 and Osh3, are also differentially phosphorylated on multiple sites suggesting that they are either involved in ceramide transfer themselves or counter-balancing its depletion by transferring other lipids³⁶.

Uncovering novel regulators of the SL pathway using functional screens

Using the temporal analysis above, we were able to distinguish cellular processes altered by myriocin. However, the majority of phosphoproteins displaying significant changes have never been proposed to be involved in SL homeostasis. Hence it was impossible to dissect from this data alone which changes were active responses, essential for regulating SL biosynthesis and which were secondary effects of the cellular changes that occurred. Since we wanted to identify novel and active regulators of the pathway, we reasoned that their presence must be important for dealing with myriocin induced SPT inhibition. We therefore decided to use functional screens to measure the ability of cells to respond to myriocin treatment in the absence or overexpression of the proteins whose phosphosites were changing (**Figure 4A**).

Our underlying hypothesis was that if a protein gets phosphorylated or dephosphorylated during myriocin treatment and this post-translational modification is an important enabler for the cell to survive under myriocin inhibition, then this protein's function must become either essential or detrimental (and the phosphorylation/dephosphorylation would be activating or repressing accordingly) during growth in myriocin. To see which proteins are either necessary or toxic during growth in myriocin we performed two systematic growth screens in yeast. We grew either a whole-genome mutant library (consisting of ~5,000 non-essential deletions¹² and ~1,000 hypomorphic alleles of essential genes¹³) or an overexpression library^{14,15} on myriocin and scored the colonies for significant changes in size relative to growth of the same strain without myriocin (for WT this ratio was close to 1) (**Figure 4A** and **Table S-2**). For this assay we chose a low myriocin concentration (0,05 µg/ml) to enable unaffected long-term growth of the WT cells, but still enabling us to capture cells with overexpressed or deleted pathway regulators (We used *Δorm2* strain as a positive control to determine optimal concentrations (data not shown)).

1
2
3
4
5
6
7
8
9
10
11
12
13
14
15
16
17
18
19
20
21
22
23
24
25
26
27
28
29
30
31
32
33
34
35
36
37
38
39
40
41
42
43
44
45
46
47
48
49
50
51
52
53
54
55
56
57
58
59
60

Next we compared the list of high-confidence regulated phosphosites at any of the time points with proteins showing an effect in the functional screens. Five deletions were both sensitive to myriocin and their deleted proteins had regulated phosphosites (Ssd1, Gph1, Shp1, Gvp36, Atg9). Four additional proteins displayed high sensitivity upon overexpression (Mlf3, Stp4, Aim21, Rod1) and had regulated phosphosites. However, in the overexpression library each yeast gene is under the control of the highly expressed and regulated GAL promoter^{14,15} that requires growth in medium containing galactose to be induced. To validate that the changes that we observed were not a result of the growth in galactose and to validate all eight of the above strains under the same metabolic conditions and relative to a WT strain, we picked all of them from the deletion library (including the strains that scored high in the overexpression library) and re-measured their growth on myriocin relative to a control (WT) strain using a more accurate, serial dilution assay (**Figure 4B**). Since regulation is often about maintaining an accurate functional balance, we found that the same regulators that affected the growth on myriocin conditions when overexpressed, also affected growth when deleted (**Figure 4B**). Since our plate assays were completely different from the original screen in their myriocin concentrations and the fact that we compared to WT (and not to own growth in the absence of myriocin), we took any deviation from the WT as a proof that the strains are differentially affected for blocking of SL biosynthesis. We thus picked for further analysis the strains that showed the strongest phenotypes on the plate assay: $\Delta gvp36$, $\Delta atg9$ that were significantly resistant to myriocin compared to WT and $\Delta stp4$ that was highly sensitive compared to WT. All these three proteins had major changes in phosphosites at early timepoints following myriocin addition (**Figure 4C**). Gvp36 is a bar domain protein³⁷, Atg9 is a transmembrane protein involved in forming autophagic vesicles through an unknown mechanism³⁸ while Stp4 is a putative transcription factor³⁹.

If indeed these proteins modulate SL biosynthesis upon myriocin treatment, the biosynthesis of SLs should be altered in their absence even at very early time points. To see the immediate effect on SL metabolism we used a 30 min pulse metabolic labeling with radioactive [4, 5 ^3H]-dihydrosphingosine which is a precursor of the SL pathway. We particularly chose pulse labeling because it allows us to follow changes in the flux in the SL pathway while longer incubation times could result in reaching an equilibrium that could mask the potential differences in regulating SL levels. We labeled cells with or without myriocin treatment and analyzed extracted lipids by thin layer chromatography (**Figure 4D**). In the case of Δstp4 we indeed saw a reduction of metabolic flow in the SL pathway that would account for its sensitivity to myriocin. Conversely, in the case of Δatg9 we see a general increase that would explain its resistance to the drug. Interestingly, in Δgvp36 there is a general reduction in mannosyl inositol phosphoryl ceramides (MIPCs) with significant decrease in phyto MIPCs, yet the strain is resistant to myriocin. This would suggest that the cause of resistance is the preservation of non-mannosylated forms (inositol phosphoryl ceramides (IPCs) and ceramides). Quantifying these changes (**Figure 4E**) shows that the loss of these proteins exerted its effect already without myriocin, suggesting that these proteins act to regulate the SL pathway not only under myriocin treatment. How these proteins regulate SL levels will require further work, but it is appealing to suggest that their phosphorylation status may play an important role in their mode of action. More generally our findings highlight the power of combining functional screens alongside phosphoproteomics in specifically recognizing proteins whose presence underlies SL homeostasis in the cells.

DISCUSSION

In our study we set out to discover new proteins involved in the maintenance of SL homeostasis. To tackle this we blocked the first committed step of *de novo* SL synthesis by employing myriocin, a highly specific inhibitor of the SPT complex, and defining changes to the transcriptome, proteome and phosphoproteome of *Saccharomyces cerevisiae* by high throughput sequencing, proteomics and phosphoproteomics. Our findings demonstrate, surprisingly, that many changes following myriocin treatment are at the post-translational steps. This is in agreement with previously published microarray analyses of changes following myriocin treatment⁴⁰. Importantly, it highlights the importance of maintaining tight SL balance in the cell to counterbalance even small changes in SL composition that can greatly influence the overall biophysical properties of membranes⁴¹. Since a response to a reduction of flow in the SL pathway by transcription, translation and transport of proteins to the site of action may take too much time and consume too much energy, immediate activation and repression of pathways seems to be carried out by posttranslational means.

Using this data we confirmed known phosphorylation sites of regulators such as Orm1 and mapped their kinetics. We were not able to identify the Orm1 phosphorylation sites that are known to be involved in controlling Orm1 activity via the TORC2 pathway upon myriocin treatment, releasing its inhibition on SPT complex (S51, S52, S53^{8,9}). Instead we found upregulated phosphorylation sites previously linked to rapamycin treatment controlling SL homeostasis by upregulating complex SL synthesis via TORC1 and nutrition sensing pathway (S29, S32, S35, S36³⁰). Since the upregulation that we observe increases over the time course of the treatment it may be that cells turn on TORC1 pathway, primarily responsible for signaling nutrition depletion, to overcome the depletion of SL. Our screen failed to uncover a number of previously described phosphosites. This discrepancy can however be readily explained by

1
2
3 differences in strategy, as our proteins were all native and untagged while previous studies used
4
5 flag-tag enrichment³⁰.
6
7

8
9 We identified and quantified phosphorylation sites for Ypk1 that had were confidently localized
10
11 to S63, S653 and S672 (Table S3). Of those, S63 and S672 were never before linked to myriocin
12
13 treatment or SL homeostasis and hence their importance in maintaining SL homeostasis needs to
14
15 be determined by further studies. Since Ypk1 directly phosphorylates the ceramide synthases,
16
17 Lag1 and Lac1¹⁰, it would be intriguing to uncover whether these phosphosites regulate this
18
19 interaction.
20
21

22
23 To sift through the hundreds of proteomic changes and decipher those that have a regulatory role
24
25 in controlling SL homeostasis, we combined the phosphoproteomics data with two functional
26
27 screens – scoring growth of strains depleted/overexpressing each yeast protein during myriocin
28
29 treatment. Our analysis enabled us to focus on three proteins that were never before suggested to
30
31 control the flux of SL biosynthesis but whose presence was indeed a determinant of SL
32
33 biosynthetic rate:
34
35

36
37 Gvp36 (Golgi Vesicle Protein of 36kDa) was first annotated in a study that used an unbiased
38
39 proteomic approach for discovering proteins that change abundance during nutritional
40
41 adaptation³⁷. Indeed $\Delta gvp36$ cells show reduced growth rate, heat and salt sensitivity, defects in
42
43 actin-cytoskeleton polarization, alterations in endocytosis and vacuolar biogenesis and defects in
44
45 entering stationary phase upon starvation³⁷. Gvp36 has a predicted BAR (Bin-Amphiphysin-Rvs)
46
47 domain similar to yeast Rvs161 and Rvs167, which were isolated because they also exhibited
48
49 reduced viability upon starvation (Rvs). Importantly, several central enzymes in the SL metabolic
50
51 pathway were discovered as suppressors of the Rvs phenotype: Sur1 the MIPC synthase, Sur2 the
52
53 4-OH LCB hydroxylase and Sur4 the fatty acid elongase. Moreover, mutations suppressing the
54
55
56
57
58
59
60

1
2
3
4
5
6
7
8
9
10
11
12
13
14
15
16
17
18
19
20
21
22
23
24
25
26
27
28
29
30
31
32
33
34
35
36
37
38
39
40
41
42
43
44
45
46
47
48
49
50
51
52
53
54
55
56
57
58
59
60

Δrvs161-related salt sensitivity all occurred in genes required for SL biosynthesis: *FEN1*, *SUR4*, *SUR2*, *SUR1*, and *IPT1*⁴². Finally, altering SL metabolism by deleting *SUR4*, reinitiates endocytosis even on a *Δrvs161* background⁴³. To this end, the two other BAR domain proteins have an obvious and tight association with SL biosynthesis suggesting that Gvp36 too might play such a central, as yet unappreciated, role. Most probably Gvp36 is also required for adaptation to nutritional changes and may be able to sense or cause changes in membranes to allow endocytosis in concert with SLs.

Atg9 (Autophagy Related 9) is a multipass transmembrane protein involved in autophagy and is conserved to humans. Atg9 was shown to be essential for formation of the phagophore assembly site (PAS). Once the autophagosome is formed, Atg9 is excluded from the vacuolar pathway and recycles into the Atg9 peripheral structures⁴⁴. Atg9 seems to have a role as a membrane carrier⁴⁵ and therefore may function in regulating autophagy during SL depletion. During autophagy Atg9 is phosphorylated directly by Atg1⁴⁶ at sites that are different than the ones we could identify. Therefore it is possible that the sites regulated by myriocin treatment are phosphorylated by a kinase other than Atg1.

Stp4 (Species-specific tRNA Processing 4) is a predicted transcription factor with two close homologs in yeast that to date does not have a defined function. It has been reported to translocate to the nucleus upon DNA replication stress induced by hydroxyurea and methyl methanesulphonate treatment⁴⁷. It may be involved in controlling SL homeostasis by sensing depletion of SLs and translocating to the nucleus to induce genes that activate the synthesis of SLs. We identified 3 phosphorylation sites (T191, S193 and S214) as significantly regulated upon myriocin inhibition.

Overall our data provide insights into dynamics of SL regulating networks and uncovers new regulators of this essential and tightly controlled metabolic pathway. The datasets presented here can and should be mined for the myriad of additional changes that exist and that may shed light on additional aspects of SL biology.

SUPPORTING INFORMATION

The Supporting information is available free of charge on the ACS Publications website <http://pubs.acs.org>

Supporting Figures

Figure S-1. Transcriptomic workflow.

Figure S-2. Effect of sphingolipid synthesis inhibition on yeast growing in various concentrations of myriocin.

Figure S-3. Qualitative evaluation of cell viability in response to low-dose of myriocin.

Figure S-4. Protein expression heatmap of proteins involved in (de)phosphorylation processes.

Figure S-5. Individual dynamic profile of Sec16 phosphorylation.

Table S-1. Transcriptomic analysis of yeast incubated in YPD medium containing 150 ng/ml or 300 ng/ml of myriocin.

Table S-2. Quantitative proteomic analysis of yeast after myriocin inhibition from 5 min to 180 min.

Table S-3. Quantitative phosphoproteomic analysis of yeast after myriocin inhibition from 5 min to 180 min.

Table S-4. Gene Ontology analysis (process, function, component) of significantly regulated phosphosites for each cluster analysis.

Table S-5. Functional analysis of cell viability after deletion or overexpression of the corresponding gene in myriocin containing medium.

ACKNOWLEDGEMENTS

Financial contributions from the Marie Curie ITN Sphingonet (project 289278, fellowships to N.L. and M.M.) are gratefully acknowledged. The proteomics part of this research was funded by the Netherlands Organization for Scientific Research (NWO) supported large-scale proteomics facility Proteins@Work (project 184.032.201). SL acknowledges support from the Netherlands Organization for Scientific Research (NWO) through a VIDI grant (project 723.013.008) and MS acknowledges the kind support of the Adelis foundation and the Kekst family institute. Maya Schuldiner is an incumbent of the Dr. Gilbert Omenn and Martha Darling Professorial Chair in Molecular Genetics. Figure 2, Figures S-1 and TOC reprinted in part with permission from: de Godoy LM, Olsen JV, de Souza GA, Li G, Mortensen P, Mann M. Status of complete proteome analysis by mass spectrometry: SILAC labeled yeast as a modelsystem. *Genome Biol.* 2006;7(6):R50 Copyright, 2006, BioMed Central.

REFERENCES

(1) Breslow, D. K. Sphingolipid homeostasis in the endoplasmic reticulum and beyond. *Cold Spring Harb. Perspect. Biol.* **2013**, 5 (4), 1–16.

(2) Futerman, A. H.; Riezman, H. The ins and outs of sphingolipid synthesis. *Trends in Cell Biology.* **2005**, 15(6), 312–8

(3) Turpin, S. M.; Nicholls, H. T.; Willmes, D. M.; Mourier, A.; Brodesser, S.; Wunderlich, C. M.; Mauer, J.; Xu, E.; Hammerschmidt, P.; Br??nneke, H. S.; et al. Obesity-induced CerS6-dependent C16:0 ceramide production promotes weight gain and glucose intolerance. *Cell Metab.* **2014**, 20 (4), 678–686.

(4) Raichur, S.; Wang, S. T.; Chan, P. W.; Li, Y.; Ching, J.; Chaurasia, B.; Dogra, S.; ??hman, M. K.; Takeda, K.; Sugii, S.; et al. CerS2 haploinsufficiency inhibits ??-oxidation and confers susceptibility to diet-induced steatohepatitis and insulin resistance. *Cell Metab.* **2014**, 20 (4), 687–695.

(5) Airola, M. V.; Hannun, Y. A. Sphingolipid metabolism and neutral sphingomyelinases. *Handb. Exp. Pharmacol.* **2013**, 215, 57–76.

(6) Epstein, S.; Riezman, H. Sphingolipid signaling in yeast: potential implications for understanding disease. *Front. Biosci. (Elite Ed).* **2013**, 5, 97–108.

(7) Nagiec, M. M.; Baltisberger, J. A.; Wells, G. B.; Lester, R. L.; Dickson, R. C. The LCB2 gene of *Saccharomyces* and the related LCB1 gene encode subunits of serine palmitoyltransferase, the initial enzyme in sphingolipid synthesis. *Proc. Natl. Acad. Sci. U. S. A.* **1994**, 91 (17), 7899–7902.

(8) Breslow, D. K.; Collins, S. R.; Bodenmiller, B.; Aebersold, R.; Simons, K.; Shevchenko, A.; Ejsing, C. S.; Weissman, J. S. Orm family proteins mediate sphingolipid homeostasis. *Nature* **2010**, 463 (7284), 1048–1053.

(9) Roelants, F. M.; Breslow, D. K.; Muir, A.; Weissman, J. S.; Thorner, J. Protein kinase Ypk1 phosphorylates regulatory proteins Orm1 and Orm2 to control sphingolipid homeostasis in *Saccharomyces cerevisiae*. *Proc. Natl. Acad. Sci.* **2011**, 108 (48), 19222–19227.

(10) Muir, A.; Ramachandran, S.; Roelants, F. M.; Timmons, G.; Thorner, J. TORC2-dependent protein kinase Ypk1 phosphorylates ceramide synthase to stimulate synthesis of complex sphingolipids. *Elife* **2014**, 3, 1–34.

(11) Fresques, T.; Niles, B.; Aronova, S.; Mogri, H.; Rakhshandehroo, T.; Powers, T. Regulation of ceramide synthase by casein kinase 2-dependent phosphorylation in *Saccharomyces cerevisiae*. *J. Biol. Chem.* **2015**, 290 (3), 1395–1403.

(12) Giaever, G.; Chu, A. M.; Ni, L.; Connelly, C.; Riles, L.; Véronneau, S.; Dow, S.; Lucau-Danila, A.; Anderson, K.; André, B.; et al. Functional profiling of the *Saccharomyces cerevisiae* genome. *Nature* **2002**, 418 (6896), 387–391.

(13) Breslow, D. K.; Cameron, D. M.; Collins, S. R.; Schuldiner, M.; Stewart-Ornstein, J.; Newman, H. W.; Braun, S.; Madhani, H. D.; Krogan, N. J.; Weissman, J. S. A comprehensive strategy enabling high-resolution functional analysis of the yeast genome. *Nat. Methods* **2008**, 5 (8), 711–718.

(14) Zhu, H.; Bilgin, M.; Bangham, R.; Hall, D.; Casamayor, A; Bertone, P.; Lan, N.; Jansen, R.; Bidlingmaier, S.; Houfek, T.; et al. Global analysis of protein activities using proteome chips. *Science* **2001**, 293 (5537), 2101–2105.

(15) Sopko, R.; Huang, D.; Preston, N.; Chua, G.; Papp, B.; Kafadar, K.; Snyder, M.; Oliver, S. G.; Cyert, M.; Hughes, T. R.; et al. Mapping pathways and phenotypes by systematic gene

- overexpression. *Mol. Cell* **2006**, *21* (3), 319–330.
- (16) Vardi, N.; Levy, S.; Gurvich, Y.; Polacheck, T.; Carmi, M.; Jaitin, D.; Amit, I.; Barkai, N. Sequential feedback induction stabilizes the phosphate starvation response in budding yeast. *Cell Rep.* **2014**, *9* (3), 1122–1134.
- (17) Langmead, B.; Trapnell, C.; Pop, M.; Salzberg, S. L. Ultrafast and memory-efficient alignment of short DNA sequences to the human genome. *Genome Biol* **2009**, *10*(3),1–10.
- (18) Gasch, A. P.; Spellman, P. T.; Kao, C. M.; Carmel-Harel, O.; Eisen, M. B.; Storz, G.; Botstein, D.; Brown, P. O. Genomic expression programs in the response of yeast cells to environmental changes. *Mol. Biol. Cell* **2000**, *11* (12), 4241–4257.
- (19) Zhou, H.; Ye, M.; Dong, J.; Corradini, E.; Cristobal, A.; Heck, A. J. R.; Zou, H.; Mohammed, S. Robust phosphoproteome enrichment using monodisperse microsphere-based immobilized titanium (IV) ion affinity chromatography. *Nat. Protoc.* **2013**, *8* (3), 461–480.
- (20) Cox, J.; Mann, M. MaxQuant enables high peptide identification rates, individualized p.p.b.-range mass accuracies and proteome-wide protein quantification. *Nat. Biotechnol.* **2008**, *26* (12), 1367–1372.
- (21) Vizcaino, J.; Deutsch, E.; Wang, R. ProteomeXchange provides globally coordinated proteomics data submission and dissemination. *Nat. ...* **2014**, *32* (3), 223–226.
- (22) Young, B. P.; Loewen, C. J. R. Balony: a software package for analysis of data generated by synthetic genetic array experiments. *BMC Bioinformatics* **2013**, *14*, 354.
- (23) Hirschberg, K.; Rodger, J.; Futerman, A. H. The long-chain sphingoid base of sphingolipids is acylated at the cytosolic surface of the endoplasmic reticulum in rat liver. *Biochem. J.* **1993**, *290* (3), 751–757.
- (24) Zanolari, B.; Friant, S.; Funato, K.; Sütterlin, C.; Stevenson, B. J.; Riezman, H. Sphingoid base synthesis requirement for endocytosis in *Saccharomyces cerevisiae*. *EMBO J.* **2000**, *19* (12), 2824–2833.
- (25) Reggiori, F.; Conzelmann, A. Biosynthesis of inositol phosphoceramides and remodeling of glycosylphosphatidylinositol anchors in *Saccharomyces cerevisiae* are mediated by different enzymes. *J. Biol. Chem.* **1998**, *273* (46), 30550–30559.
- (26) Wadsworth, J. M.; Clarke, D. J.; McMahon, S. A.; Lowther, J. P.; Beattie, A. E.; Langridge-Smith, P. R. R.; Broughton, H. B.; Dunn, T. M.; Naismith, J. H.; Campopiano, D. J. The chemical basis of serine palmitoyltransferase inhibition by myriocin. *J. Am. Chem. Soc.* **2013**, *135* (38), 14276–14285.
- (27) Iwaki, S.; Kihara, A.; Sano, T.; Igarashi, Y. Phosphorylation by Pho85 cyclin-dependent kinase acts as a signal for the down-regulation of the yeast sphingoid long-chain base kinase Lcb4 during the stationary phase. *J. Biol. Chem.* **2005**, *280* (8), 6520–6527.
- (28) Zhang, X.; Lester, R. L.; Dickson, R. C. Pil1p and Lsp1p negatively regulate the 3-phosphoinositide-dependent protein kinase-like kinase Pkh1p and downstream signaling pathways Pkc1p and Ypk1p. *J. Biol. Chem.* **2004**, *279* (21), 22030–22038.
- (29) de Graaf, E. L.; Giansanti, P.; Altelaar, A. F. M.; Heck, A. J. R. Single-step enrichment by Ti4+-IMAC and label-free quantitation enables in-depth monitoring of phosphorylation dynamics with high reproducibility and temporal resolution. *Mol. Cell. Proteomics* **2014**, *13* (9), 2426–2434.
- (30) Shimobayashi, M.; Oppliger, W.; Moes, S.; Jenö, P.; Hall, M. N. TORC1-regulated protein kinase Npr1 phosphorylates Orm to stimulate complex sphingolipid synthesis. *Mol. Biol. Cell* **2013**, *24*, 870–881.

- (31) Aronova, S.; Wedaman, K.; Aronov, P. A.; Fontes, K.; Ramos, K.; Hammock, B. D.; Powers, T. Regulation of Ceramide Biosynthesis by TOR Complex 2. *Cell Metab.* **2008**, 7 (2), 148–158.
- (32) Holt, L. J.; Tuch, B. B.; Villén, J.; Johnson, A. D.; Gygi, S. P.; Morgan, D. O. Global analysis of Cdk1 substrate phosphorylation sites provides insights into evolution. *Science* **2009**, 325 (5948), 1682–1686.
- (33) Kamada, Y.; Fujioka, Y.; Suzuki, N. N.; Inagaki, F.; Wullschleger, S.; Loewith, R.; Hall, M. N.; Ohsumi, Y. Tor2 directly phosphorylates the AGC kinase Ypk2 to regulate actin polarization. *Mol. Cell. Biol.* **2005**, 25 (16), 7239–7248.
- (34) Jesch, S. A.; Gaspar, M. L.; Stefan, C. J.; Aregullin, M. A.; Henry, S. A. Interruption of inositol sphingolipid synthesis triggers Stt4p-dependent protein kinase C signaling. *J. Biol. Chem.* **2010**, 285 (53), 41947–41960.
- (35) Horvath, A.; Sütterlin, C.; Manning-Krieg, U.; Movva, N. R.; Riezman, H. Ceramide synthesis enhances transport of GPI-anchored proteins to the Golgi apparatus in yeast. *EMBO J.* **1994**, 13 (16), 3687–3695.
- (36) Kajiwar, K.; Ikeda, A.; Aguilera-Romero, A.; Castillon, G. A.; Kagiwada, S.; Hanada, K.; Riezman, H.; Muniz, M.; Funato, K. Osh proteins regulate COPII-mediated vesicular transport of ceramide from the endoplasmic reticulum in budding yeast. *J Cell Sci* **2014**, 127 (Pt 2), 376–387.
- (37) Querin, L.; Sanvito, R.; Magni, F.; Busti, S.; Van Dorsselaer, A.; Alberghina, L.; Vanoni, M. Proteomic analysis of a nutritional shift-up in *Saccharomyces cerevisiae* identifies Gvp36 as a BAR-containing protein involved in vesicular traffic and nutritional adaptation. *J. Biol. Chem.* **2008**, 283 (8), 4730–4743.
- (38) Chang, C.-Y.; Huang, W.-P. Atg19 Mediates a Dual Interaction Cargo Sorting Mechanism in Selective Autophagy. *Mol. Biol. Cell* **2007**, 18, 919–929.
- (39) Y. Yang, Z. Zhang, Y. Li, X.-G. Zhu, Q. L. Identifying cooperative transcription factors by combining ChIP-chip data and knockout data. *Cell Res.* **2010**, 20, 1216–1278.
- (40) Montefusco, D. J.; Chen, L.; Matmati, N.; Lu, S.; Newcomb, B.; Cooper, G. F.; Hannun, Y. a; Lu, X. Distinct signaling roles of ceramide species in yeast revealed through systematic perturbation and systems biology analyses. *Sci. Signal.* **2013**, 6 (299), rs14.
- (41) Holthuis, J. C. M.; Menon, A. K. Lipid landscapes and pipelines in membrane homeostasis. *Nature* **2014**, 510 (7503), 48–57.
- (42) Balguerie, A.; Bagnat, M.; Bonneu, M.; Aigle, M.; Breton, A. M. Rvs161p and sphingolipids are required for actin repolarization following salt stress. *Eukaryot. Cell* **2002**, 1 (6), 1021–1031.
- (43) Morgan, J.; McCourt, P.; Rankin, L.; Swain, E.; Rice, L. M.; Nickels, J. T. Altering sphingolipid metabolism in *saccharomyces cerevisiae* cells lacking the amphiphysin ortholog rvs161 reinitiates sugar transporter endocytosis. *Eukaryot. Cell* **2009**, 8 (5), 779–789.
- (44) Backues, S. K.; Orban, D. P.; Bernard, A.; Singh, K.; Cao, Y.; Klionsky, D. J. Atg23 and Atg27 Act at the Early Stages of Atg9 Trafficking in *S. cerevisiae*. *Traffic* **2015**, 16 (2), 172–190.
- (45) He, C.; Klionsky, D. J. Atg9 trafficking in autophagy-related pathways. *Autophagy* **2007**, 3 (3), 271–274.
- (46) Papinski, D.; Schuschnig, M.; Reiter, W.; Wilhelm, L.; Barnes, C. A.; Maiolica, A.; Hansmann, I.; Pfaffenwimmer, T.; Kijanska, M.; Stoffel, I.; et al. Early Steps in Autophagy Depend on Direct Phosphorylation of Atg9 by the Atg1 Kinase. *Mol. Cell* **2014**, 53 (3), 471–483.
- (47) Tkach, J. M.; Yimit, A.; Lee, A. Y.; Riffle, M.; Costanzo, M.; Jaschob, D.; Hendry, J. A.; Ou, J.;

Moffat, J.; Boone, C.; et al. Dissecting DNA damage response pathways by analysing protein localization and abundance changes during DNA replication stress. *Nat. Cell Biol.* **2012**, *14* (9), 966–976.

- (48) Kulak, N. A.; Pichler, G.; Paron, I.; Nagaraj, N.; Mann, M. Minimal, encapsulated proteomic-sample processing applied to copy-number estimation in eukaryotic cells. *Nat. Methods* **2014**, *11* (3), 319–324.

FIGURE LEGENDS

Figure 1. Transcriptome analysis of low dose myriocin treated cells.

A. Outline of the different methods used to study sphingolipid metabolism in yeast. B. Transcriptome analysis of up and downregulated genes. Yeast grown in YPD were supplemented with two concentrations of myriocin (150 ng/ml and 300 ng/ml). Duplicate samples were taken at 0 and 60 min and subjected to deep sequencing. Transcripts were quantified and the changes in the number of transcripts at 60 min were compared to that of 0 min and plotted. The two fold up- and down-regulated transcripts that belong to the SL pathway are indicated with red and green font colors, respectively. C. Sphingolipid metabolic pathway. Shown are the enzymatic steps, enzymes (black, red or green) and selected regulators (grey filled circle) of the sphingolipid pathway. Upregulated transcripts at 150 ng/ml myriocin treatment are indicated in red while downregulated transcripts are indicated in green. D. Quantitative analysis of up- and down-regulated transcripts. The number of regulated transcripts at 60 min compared to 0 min at different concentrations of treatment are indicated.

Figure 2. In-depth proteomic analysis of low dose myriocin treated cells.

A. (Phospho)proteomic workflow. Yeast were grown in YPD medium until mid-log phase ($OD_{600}=0.8$) and collected after incubation with 150 ng/ml myriocin inhibitor for 5, 30, 60, 120 and 180 min. 3 biological replicates were analyzed per condition. Cells were lysed and proteins digested into peptides by trypsin and Lys-C. Samples were submitted to nanoLC-MS/MS analysis in a technical duplicate and protein quantification was performed by label-free using Maxquant. In parallel, the same samples were subjected to Ti^{4+} -IMAC tips phosphopeptide enrichment. Phosphopeptides were analyzed in a technical duplicate by nanoLC-MS/MS. Phosphosites were quantified by label-free quantification using Maxquant to determine potent regulatory sites in sphingolipid homeostasis. B. Quantitative yeast proteome analysis after incubation with myriocin inhibitor. The histogram displays the number of up and downregulated proteins per time point. The number of regulated proteins is drastically increasing after 120 min of myriocin inhibition with a maximum of 385 regulated proteins after 180 min. C. Integration of quantitative transcriptomic and proteomic analysis. Correlation between mRNA ratios (y-axis) and protein ratios (x-axis) after 60 min of myriocin inhibition. The quantified proteins known to be involved in the sphingolipid metabolism (yellow) do not display significant regulation. Most of the up-regulated genes (in red) are associated with the general stress response. D. Protein expression heatmap of sphingolipid metabolic pathway related proteins. For every time point the color scale is depicting the Log_2 protein ratio. SPOTS complex members including Lcb1, Lcb2 and Sac1 are up-regulated in late time.

Figure 3. In-depth phosphoproteomic analysis unravels potential regulatory sites involved in sphingolipid homeostasis.

A. Individual dynamic profiles of phosphoproteins controlling sphingolipid metabolism. Dynamic representation of Log₂ ratio for the regulated sites belonging to 3 selected phosphoproteins known to control *de-novo* synthesis of sphingolipids. The histogram (in black) represents the Log₂ protein ratio of the selected phosphoprotein for each time points. Ypk1 was not quantified at the protein level. Orm1 S32-3 and S36-3 correspond to the S32 and S36 ORM1 phosphosites quantified from a triply phosphorylated peptide. B. Quantitative yeast phosphosite analysis. A total of 6219 unique phosphorylation sites were quantified in at least 2 biological replicates using Maxquant. Of those, 996 showed a significant regulation of at least 4 fold change after myriocin inhibition in at least one time point. Regulated phosphosites were distributed by Euclidian distance according to 6 different clusters. The blue line represents the averaged trend of the specified cluster. C. Enriched GO functions of regulated phosphoproteins of 3 clusters. Graphical representation of GO enriched functions. Y-axis is displaying the statistical significance of enrichment as evaluated by the p-value while the x-axis displays the ranking of the enriched GO function according to the p-value (x-axis).

Figure 4. Biological verification of newly identified proteins on SL homeostasis.

A. Functional screens. A whole-genome mutant library (consisting of ~5,000 non-essential deletions¹² and ~1,000 hypomorphic alleles of essential genes¹³) or an overexpression library (where each yeast gene is under control of the highly expressed and regulated GAL promoter^{14,15}) were grown on myriocin and the colonies were scored for changes in size. Based on the growth phenotype and phosphoproteome analysis we chose genes for further analysis. B. Validation of hits by dilution assays. Serial dilution of the indicated strains were spotted on agar plates containing 0 or 1,000 ng/ml myriocin and imaged after 48-72h of growth. C. Individual dynamic profiles of the most interesting regulated phosphoproteins. Dynamic representation of Log₂ ratio for the regulated sites belonging to 3 selected phosphoproteins. The histogram (in black) represents the Log₂ protein ratio of the selected phosphoprotein for each time points. ATG9 and STP4 were not quantified at the protein level. D. Metabolic labeling of regulators. Cultures of the indicated strains in exponential phase were incubated with [4, 5 ³H]-dihydrosphingosine for 30 min. Lipids were extracted, separated on thin layer chromatography (A representative image of three independent experiment is shown.) E. Quantification of metabolic labeling. Quantification of three independent experiments of metabolic labeling. Values are normalized to wild type. Asterisks show statistical significance (* p< 0.05, ** p<0.01).

A



Figure 3

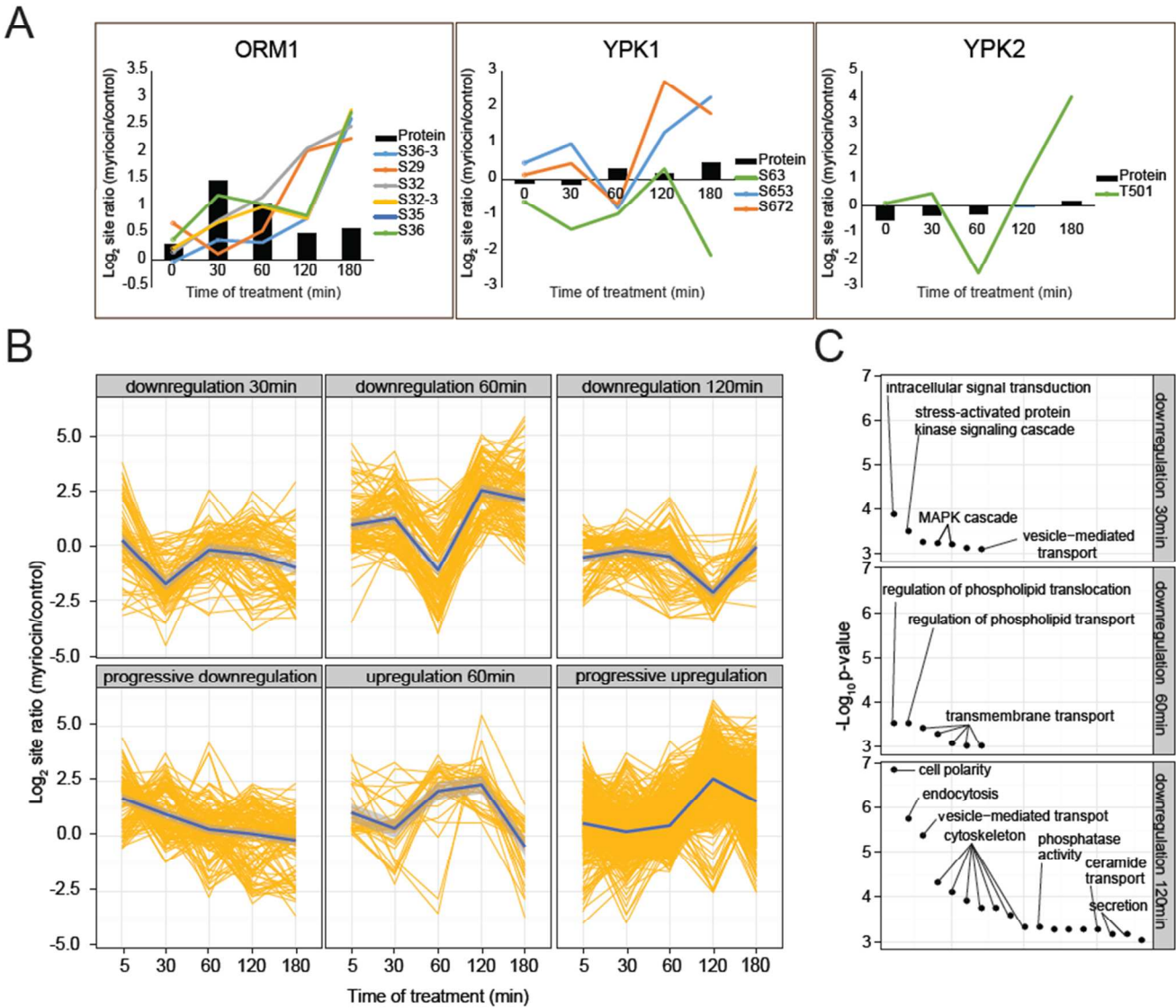
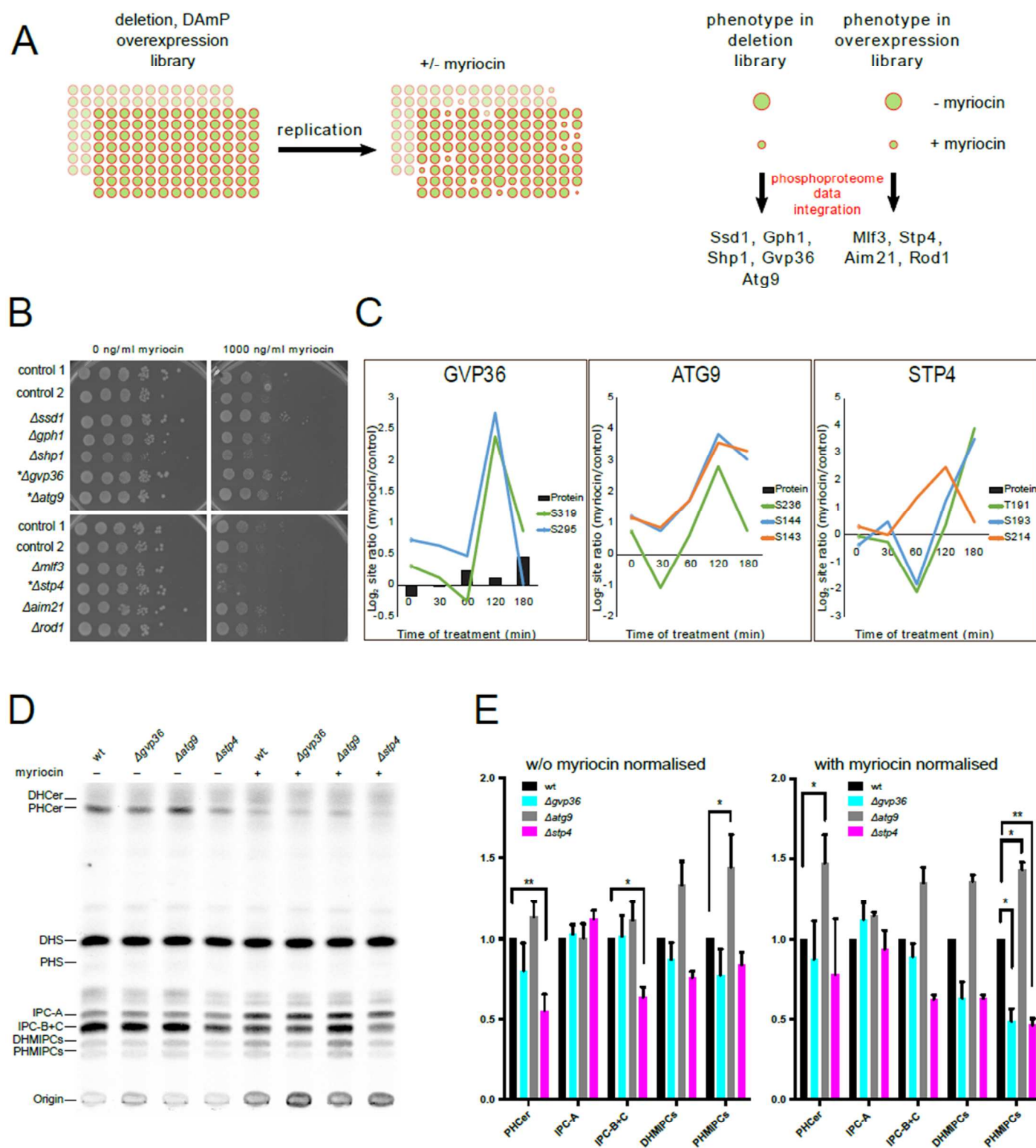


Figure 4



for TOC only

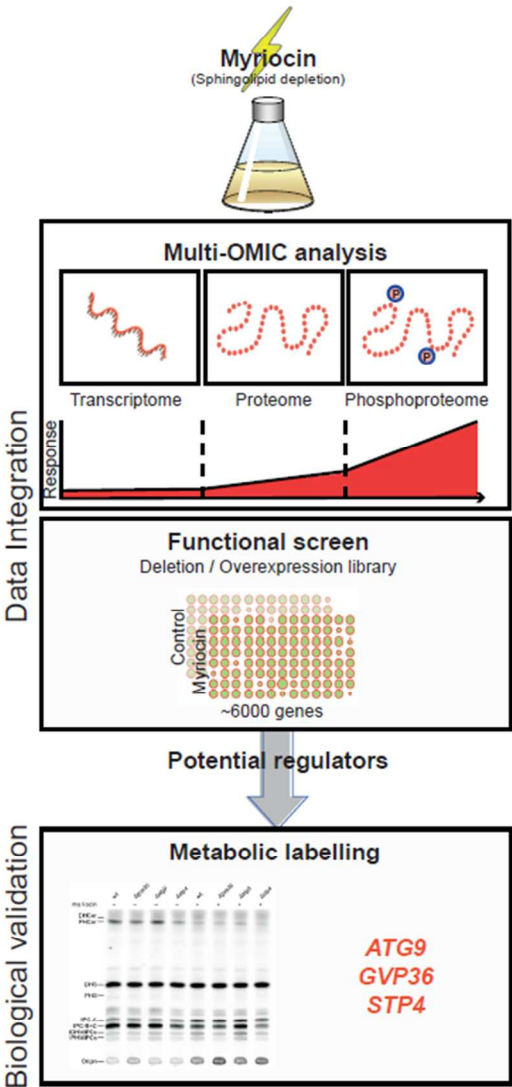


Image courtesy of N. Lebesgue, Copyright 2016